AGU PUBLICATIONS

Geochemistry, Geophysics, Geosystems

RESEARCH ARTICLE

10.1002/2016GC006756

Key Points:
- Rock magnetic experiments and magnetic survey were first integrated to investigate the vein-type uranium deposits
- Magnetic properties of the ore body and the wall rocks change gradually from the margin to the center of the veins
- Rock magnetic analyses of uranium deposits are significant for their magnetic survey responses

Supporting Information:
- Supporting Information S1

Correspondence to:
K. Ge,
kunpeng.ge@yahoo.com

Citation:
Ge, K., Q. Liu, J. Deng, D. Nobes, Y. Wang, Y. Wang, and X. Chen (2017), Rock magnetic investigation and its geological significance for vein-type uranium deposits in southern China, *Geochem. Geophys. Geosyst.*, *18*, 1333–1349, doi:10.1002/2016GC006756.

Received 1 DEC 2016
Accepted 3 MAR 2017
Accepted article online 7 MAR 2017
Published online 1 APR 2017

© 2017. American Geophysical Union. All Rights Reserved.

Rock magnetic investigation and its geological significance for vein-type uranium deposits in southern China

Kunpeng Ge[1,2], Qingsong Liu[3,4], Juzhi Deng[1,2], David Nobes[1], Yang Wang[5], Yanguo Wang[1], and Xiao Chen[1]

[1]School of Geophysics and Measurement-control Technology, East China University of Technology, Nanchang, China, [2]Fundamental Science on Radioactive Geology and Exploration Technology Laboratory, East China University of Technology, Nanchang, China, [3]Department of Marine Science and Engineering, Southern University of Science and Technology of China, Shenzhen, China, [4]Laboratory for Marine Geology, Qingdao National Oceanography Laboratory for Marine Science and Technology, Qingdao, China, [5]Guangdong Province Nuclear Industry Geology Bureau 293 Dadui, Guangzhou, China

Abstract To characterize the metallogenic environment of a typical vein-type uranium deposit, samples from diabase dykes, alteration zones including metamorphic diabase and uranium ore, and granites were systematically investigated for six boreholes from southeastern China. Rock magnetic results indicate that coarse-grained magnetites (pseudosingle domain, PSD, and multidomain, MD) are dominant magnetic carriers in diabase. In contrast, the uranium ore is dominated by fine-grained magnetites (superparamagnetic, SP, and single-domain, SD). The concentration of magnetic particles in fresh granites is low. Magnetic properties of metamorphic diabases exhibit much greater variability of magnetic properties and higher degrees of sulfuration than unaltered diabase and granite, due to contact metasomatism and reduction effects close to the vein. Compared with diabase, magnetic remanence of the uranium ore is much lower, but displays much higher stability. The Koenigsberger ratio Q peaks in the uranium ore with a value of $\sim$1.00. Using the systematic rock magnetic results to constrain the interpretation, the contribution of the intersection zone of diabase dyke and silicified fault to magnetic anomalies was further modeled, and the effects of the ore body are significant for magnetic exploration. Overall, rock magnetic investigations of vein-type uranium deposit provide a better understanding of the interactions between different rock types, and further facilitate regional magnetic surveys on the ground.

1. Introduction

As an economical, industrial, and strategic mineral resource, exploration of uranium deposits has been attracting much attention [*US Atomic Energy Commission*, 1974; *Ruzicka*, 1993; *Castor and Henry*, 2000]. Several types of uranium deposits have been identified since the beginning of uranium ore prospecting such as vein-type, sandstone-hosted type, uranium-bearing coal type, and carbonate-siliceous-argillitic type [*Nettleton*, 1976; *Castor and Henry*, 2000]. Among them, the vein-type occurs worldwide, and most often in the geological settings of a folded belt and a tectonically active region [*Cunningham et al.*, 1998; *Marignac and Cuney*, 1999]. In China, the hydrothermal uranium deposit that has been generated in the contact metamorphic zone is one of the most prominent vein-type deposits [*Hu et al.*, 2008], e.g., the Xiangshan volcanic-type hydrothermal deposit and the Xiazhuang granite-type alkaline hydrothermal deposit. The Xiazhang uranium deposit is controlled by a swarm of intersecting diabase dykes, with nearly EW-strike, and a silicified fault system with NNE-extension, hence the nomenclature for the "intersection-type" of uranium deposit. From an economic geology viewpoint, the orebodies in these typical vein-type uranium deposits are characterized by their concentrated distribution, large reserves, as well as simple ore composition, high-grade, and leachability of uranium, and hence possess good potential for mining [*Cuney and Barbey*, 2014].

Geophysical methods, including radiometric, magnetic, gravimetric, magnetotelluric, and seismic prospecting, have been conducted for uranium deposit exploration [*Chen et al.*, 2012; *Cuney and Barbey*, 2014; *WoldeGabriel et al.*, 2014]. In particular, radioactivity prospecting, including the airborne and car-borne gamma-spectrometric survey, and soil-mercury-survey are the direct prospecting methods for uranium exploration, but are only valid for shallow orebodies with depths less than 100 m [*Saunders et al.*, 1987; *Reynier* *et al*., 2015]. The other geophysical methods can only provide indirect prospecting information for uranium deposits [*Castor and Henry*, 2000].

However, with continuing consumption of the shallow uranium ore, the investigation of uranium deposits has now shifted to deeper blind ore prospecting stage [*Boyle*, 2013]. Deep-seated large-scale magmatic activity is an important factor for further uranium concentration, and the deep-seated faults are favorable passage-ways for migration of uranium ore-forming fluid [*Shu*, 2004; *Tuncer et al*., 2006; *Orozco et al*., 2013], which can be located by geophysical methods. Furthermore, some characteristics of geophysical fields could reflect the ore-forming geological environments relevant to uranium mineralization. For example, uranium deposits can be located in underground paleochannels [*Bonnetti et al*., 2015], and in the depression of a Moho discontinuity [*Shu*, 2004], both of which always have low gravity fields.

Hydrothermal demagnetization is an important characteristic of uranium precipitation from ore-forming fluids. It can change magnetic minerals to nonmagnetic minerals during the metamorphism, making magnetic exploration more difficult when exploring for vein-type uranium deposits [*Min et al*., 2005]. The inherent nonuniqueness of the geophysical inversion is exacerbated by limited constraints and observational data [*Nettleton*, 1976; *Hinze et al*., 2013]. Therefore, more details about the physical properties of the target (e.g., susceptibility, density, resistivity, seismic velocity, gamma ray spectrum) are required to constrain the geophysical observation [*Shenoy et al*., 1972; *Wachter and Cremers*, 1987].

Studies on physical properties of rocks related to uranium deposition have been conducted together with the development of uranium resources [*Shenoy et al*., 1972; *Wachter and Cremers*, 1987; *Min et al*., 2005]. In particular, it has been shown that the physical properties vary gradually from the centers of the veins to the margins [*Wang et al*., 2010; *Boyle*, 2013].

Compared with traditional geophysical measurements, rock magnetic experiments including magnetic susceptibility and magnetic hysteresis have the advantages of high efficiency and low costs [*Thompson and Oldfield*, 1986]. They have been successfully applied in a wide range of geological and environmental processes [*Tauxe et al*., 2002; *Zhu et al*., 2004; *Roberts*, 2006; *Liu et al*., 2012]. In addition, they have already been applied in researching deposit exploration and development since 1980s [*Dunlop and Özdemir*, 2001]. For instance, the susceptibilities of ferromagnetic minerals are thought to vary gradually under the influence of hydrocarbons [*Liu et al*., 2000]. Therefore, the mineralization zone could be delineated by comprehensively analyzing the source and formation mechanism of magnetic grains.

In this study, we will investigate the typical vein-type uranium deposit in the Xiazhuang field by a comprehensive rock magnetic approach. Since the Xiazhuang mine region is an old prospecting area, significant exploration results have already been obtained from geological and geophysical studies [*Wu et al*., 2003; *Yang*, 2009; *Chen et al*., 2012; *Cuney and Barbey*, 2014; *WoldeGabriel et al*., 2014]. These previous results provide solid background information for this study. The resulting properties of the vein-type uranium deposit will be combined with forward modeling to provide a basis for interpreting geophysical surveys in this area.

2. Geological Setting and Sampling

The Xiazhuang uranium ore field is located in the eastern part of Guidong massive granite body, situated on the western margin of Cathaysia block [*Hu et al*., 2008; *Chen et al*., 2012; *Cuney and Barey*, 2014; *Pownceby and Johnson*, 2014] (Figure 1). The sampling area is conformably overlain by medium grained porphyritic granite intruded at the first Yanshanian stage, and is coupled with the late intruded and widely outcropping mafic dykes [*Hu et al*., 2008]. Geological and geochemical studies have shown that the Guidong granite body experienced multiple episodes of melting during the Indosinian-Yanshan tectonic movement [*Wang*, 2010; *WoldeGabriel et al*., 2014]. The diabase dykes are distributed in a NWW direction, while the structural belts (e.g., silicified faults) are also highly developed, and aligned NNE. The vein-type uranium mineralized in an integrated system, i.e., the trinity of the reducing diabase, surrounding uranium-enriched granite and the rising thermal fluids in fracture zones, is considered to originate from a mixture of consolidated acid igneous rocks and uranium enriched mantle [*Hu et al*., 1993]. The uranium deposits are controlled by the junctions of the diabase dykes and the silicified faults, where strong metamorphism and metasomatism occurs. Numerous boreholes have been designed around these intersections for harvesting the uranium ores.

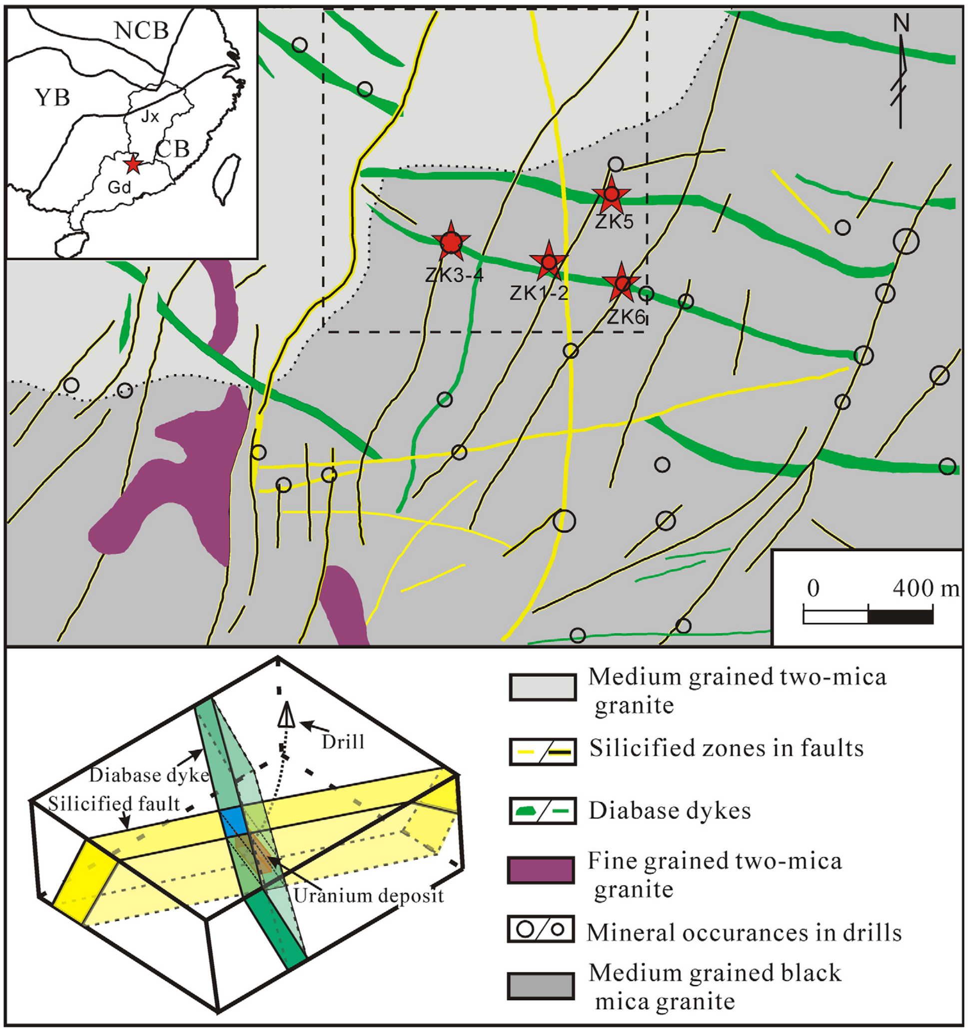

Figure 1. Geological sketch map of Xiazhuang area. A map of Southeast China showing the location of Xiazhang area, sited at the boundary of Jiangxi province (Jx) and Guangdong province (Gd), is inserted for illustrative purpose. The area in dashed square (1000 m × 1000 m) was selected for magnetic survey. The sketch map of the intersection zone that contains a uranium deposit is shown in the left bottom. The labeled stars indicate the sample borehole locations. Abbreviated symbols: NCB = North China block; YB = Yangtze block, CB = Cathaysian block.

We collected samples from six representative boreholes (ZK1-6 in Figure 1). The central zones of boreholes, where the orebody appeared, are around the deep intersection position of the NWW-aligned diabase dykes and the NNE-aligned silicified faults (Figure 1). The sampling sequence was diabase, weakly altered diabase, uranium ore, and granite, respectively (hereinafter separately referred to as samples Db, Mb, Uo, and Gn). To ensure the accuracy of measurements, replicate samples in these boreholes were also collected for each type of rock. From the collected rock samples, small cylindrical specimens were drilled with diameters of ~0.4 cm and heights of ~0.6 cm. The specimens were divided into two groups for rock magnetic and paleomagnetic measurements. The remaining fresh off-cuts were collected for microscope investigations.

3. Methods

3.1. Rock Magnetic Measurements

Hysteresis parameters, isothermal remanent magnetization (IRM) acquisition curves, and the first-order reversal curves (FORC) of representative specimens were measured using a vibrating sample magnetometer (VSM, Princeton Measurements Corp., New Jersey, USA) at room temperature with field range of ±1 T. Saturation remanence (M_{rs}), saturation magnetization (M_s), and coercivity (B_c) were determined after correction for the high-field paramagnetic contribution. Subsequently, saturation IRM (SIRM) was obtained using an applied field up to 2 T, and then demagnetized in a stepwise back-field to determine the coercivity of remanence (B_{cr}).

To characterize the magnetic minerals in samples, temperature-dependent magnetic susceptibility curves (χ-T) were measured using the multifunctional Kappabridge (MFK, Agico Ltd., Brno, Czech Republic), from room temperature to 700°C in an argon atmosphere (at an Ar flux rate of 100 mL/min) in a field of 200 Am^{-1}, using a frequency of 976 Hz.

Three-axis IRM demagnetization experiments [*Lowrie*, 1990] were conducted to investigate the components and concentration of magnetic minerals in selected samples. After magnetization in the 2.5 T field along the sample Z axis, a 0.5 T field was applied along the sample Y axis and a 0.15 T field along the sample X axis [*Lowrie*, 1990]. Samples were then thermally demagnetized in a stepwise fashion with a magnetic measurement thermal demagnetizer super-cooled (MMTDSC) oven designed by John Shaw [*Hill and Shaw*, 1999], and then measured with the 2G-760 superconducting quantum interference device magnetometer (SQUID, 2G Corp., Mountain View, USA) after each step.

Low-temperature magnetic behaviors were investigated using a quantum design magnetic property measurement system (MPMS, Princeton Measurements Corp., New Jersey, USA). Representative specimens were first cooled to 10 K in a zero field magnetic field, imparted a SIRM in a pulse field of 2.5 T, and then warmed to 300 K in a zero field.

3.2. Paleomagnetic Measurements

Remanent magnetizations and alternating field (AF) demagnetizations were measured using the 2G-760 SQUID magnetometer. Specimens were subjected to stepwise AF demagnetization in 13 steps up to 80 mT. The resulting decay pattern of the remanence was displayed in orthogonal projections [*Zijderveld*, 1967; *Kirschvink*, 1980], and the directions of the remanence components were plotted using PMGSC [*Enkin and Dunlop*, 1987].

3.3. Mineralogy Investigation

Microscope investigation is necessary to understand the diagenetic processes that have affected the rocks, and is also a useful method to identify the mineral species [*Liu et al*., 2011]. To investigate the microtexture directly and verify the implications from magnetic measurements, polished thin sections of selected samples were studied under an ECLIPSE LV100N POL polarizing microscope (Nikon Corp., Tokyo, Japan).

3.4. Forward Modeling

On the basis of the geological setting and the obtained averaged magnetic parameters of the intersection-type structure, forward models of various combinations of sample Db, Mb, Uo, and Gn were constructed to reproduce the magnetic anomalies on the ground. Intersection zones were modeled by simply superimposed anomalies of different magnetized parallelepipeds [*Shen and Guan*, 1985, refers to the supporting information S1]. For simplicity, all types of rocks are supposed to have bedding induced (M_i) and remanent magnetization (M_r). It means the direction of magnetization M ($M = M_i + M_r$) oriented in the plane of diabase dyke, and the horizontal component M is parallel to dip of the dyke. In addition, given that all models are surrounded by the wall rocks (Sample Gn), the anomalies due to the wall rocks have been simply subtracted. The programs used to calculate the magnetic anomalies are summarized in the supporting information S1.

4. Results

4.1. Rock Magnetic Results

The statistical magnetic properties of collected samples vary as a function of the sampling sequence, i.e., from sample Db to sample Gn (Figure 2). Magnetic parameters, for example, the susceptibility and remanence, decrease continuously from rim to center of the veins, while coercivities and the values of the Koenigsberger ratio Q (the ratio of remanent magnetization to induced magnetization) of sample Uo are much larger than other types of rocks [*Koenigsberger*, 1938]. The wall rock (sample Gn) possesses the lowest magnetic parameters. Overall, with the exception of relatively greater variations of magnetic parameters for

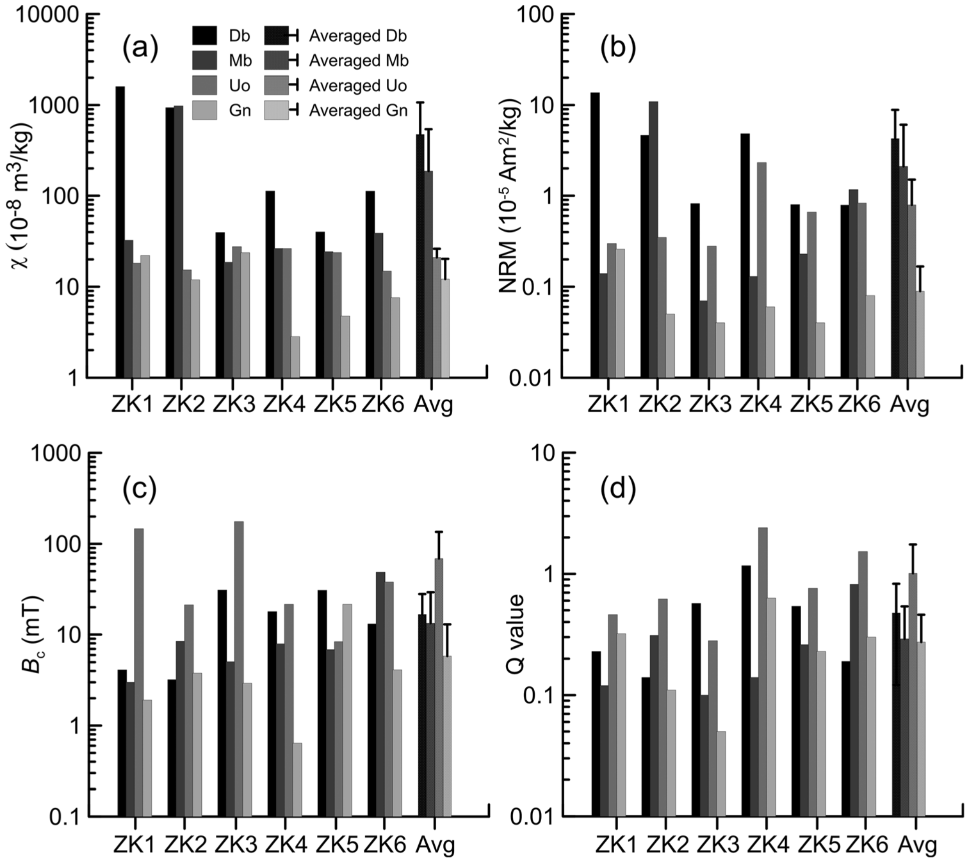

Figure 2. Variations of comprehensive magnetic properties, i.e., (a) susceptibility, (b) NRM, (c) coercivity, and (d) the Koenigsberger ratio Q for four types of samples in different boreholes. The averaged values (Avg) and error bars (one standard deviation) of magnetic properties for six boreholes are also displayed respectively in subgraphs.

samples Mb, series of samples from different boreholes display similar magnetic characteristics from rim to center of the veins.

Hysteresis loops, and IRM component analyses that are obtained by decomposing the IRM acquisition curves to sets of log-Gaussian curves are shown in Figure 3 [*Kruiver et al*., 2001]. Sample Db displays pseudo-single domain (PSD) or multidomain (MD) behaviors after a paramagnetic correction (Figure 3e). The dominant magnetic component of Sample Db (Figure 3i) shows mean coercivity at half distribution width ($B_{1/2}$) of 28.2 mT, while the second component ($B_{1/2} = 354.8$ mT) is also evident. Compared with sample Db, sample Mb (Figures 3b and 3f) displays higher coercivity (B_c) and M_{rs}/M_s ratio, but decreased magnetization. The primary component of sample Mb is similar to that for sample Db, whereas the corresponding second magnetic component is almost undetectable (Figure 3j).

The magnetization of sample Uo is dominated by paramagnetic minerals (Figure 3c). However, the remaining ferromagnetic minerals have pronounced wasp-waisted hysteresis loops and higher B_c value. IRM analysis of sample Uo also shows two distinct components, with $B_{1/2}$ of 44.7 mT and 2818.4 mT, respectively. Sample Gn (granite) displays decreased B_c, with less amount of ferromagnetic minerals in comparison with diabases samples. The dominant ferromagnetic component of sample Gn shows a $B_{1/2}$ of 20 mT.

FORC diagrams provide a means of separating different magnetic contributions in terms of coercivites and interaction fields. As is shown in Figure 4, FORC diagram of sample Db exhibited small central B_c, while extensions of contours to axis of B_u are observed. In contrast to sample Db, much closed concentric contours along B_u occur for sample Mb, while the distribution of B_c still exists. Compared with sample Mb, sample Uo has a more narrow vertical (magnetic interaction) distribution, but more extended horizontal (coercivity, $>$100 mT) distribution. The FORC contours of sample Gn display a peak closed to the origin, accompanied by significant noise.

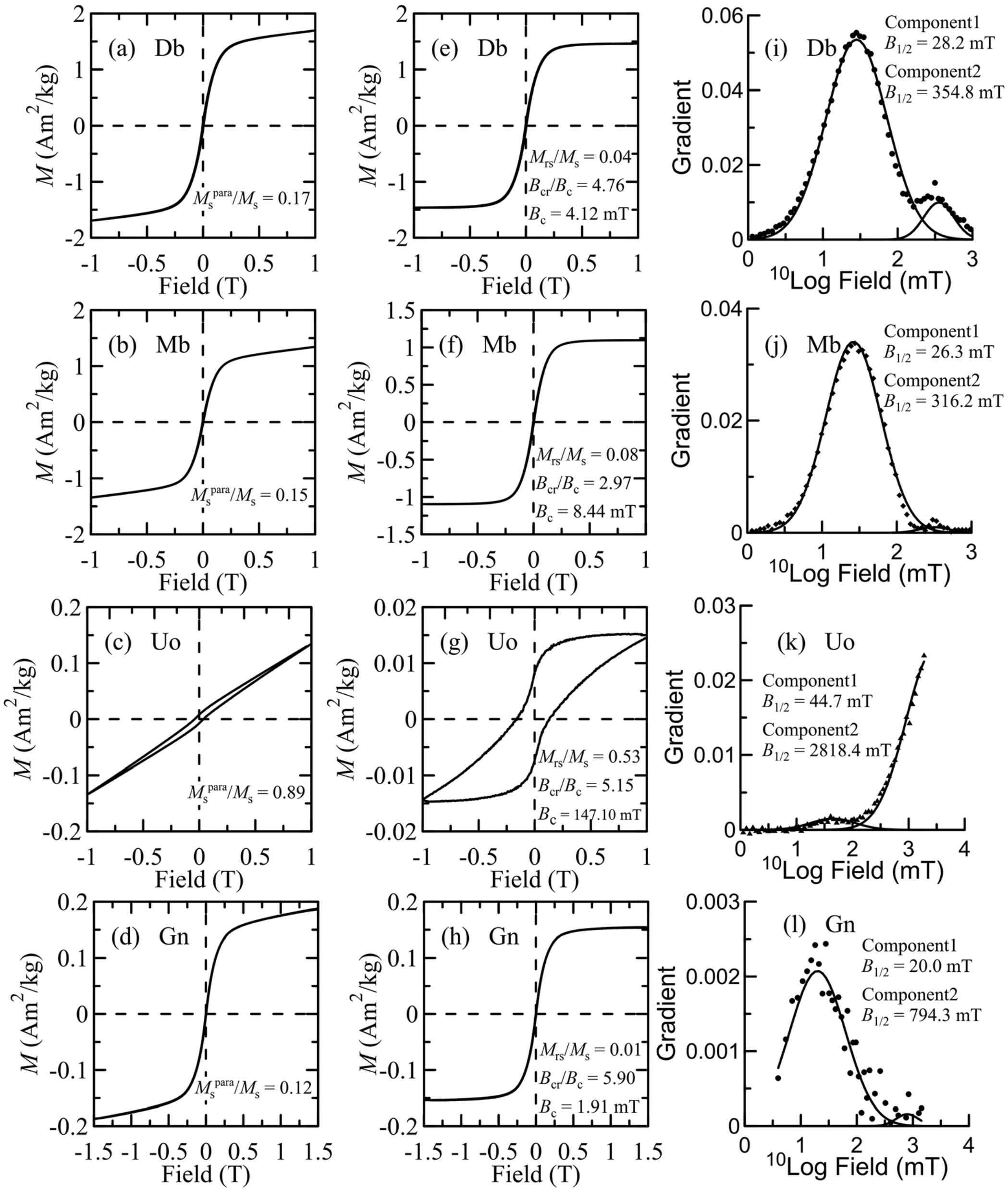

Figure 3. (a–d) Representative hysteresis loops of samples from borehole ZK1 before and (e–h) after paramagnetic correction, and (i–l) IRM component analyses curves of four selected samples, namely Db, Mb, Uo, and Gn. M_s^{para}/M_s: The ratio of magnetization contributed by paramagnetic minerals at the saturated magnetic field to M_s.

The χ-T curves show a clear drop at about 585°C for all selected samples (Figure 5). In particular, sample Db displays fairly smooth trends of the heating curve before 585°C (Figures 5a and 5e). The cooling curves are almost reversible with respect to their heating curves, with the exception of sample Db-3 in Figure 5i. It is notable that the magnetic properties of sample Mb show the largest variation between different boreholes. The smooth heating curve still exists (Figure 5f), but samples from other boreholes (Figures 5b and 5j) display a much smaller and gradually decreasing susceptibility as a function of temperature, and reaches a Hopkinson peak [*Hopkinson*, 1889] before its unblocking temperature. The χ-T curves for these samples are not reversible, and the cooling branches peak at 300–400°C. For sample Uo, the initial susceptibility (Figures 5c, 5f, and 5k) decreases remarkably in comparison with samples Db and Mb. Nevertheless, a drop can still be easily distinguished at about 585°C. The susceptibility of granite (Figures 5d, 5h, and 5l) decreases gradually before ~500°C, then reaches a remarkable Hopkinson peak, and fall at about 585°C. The fluctuations after 585°C for samples Gn are probably noise [*Hrouda*, 2011].

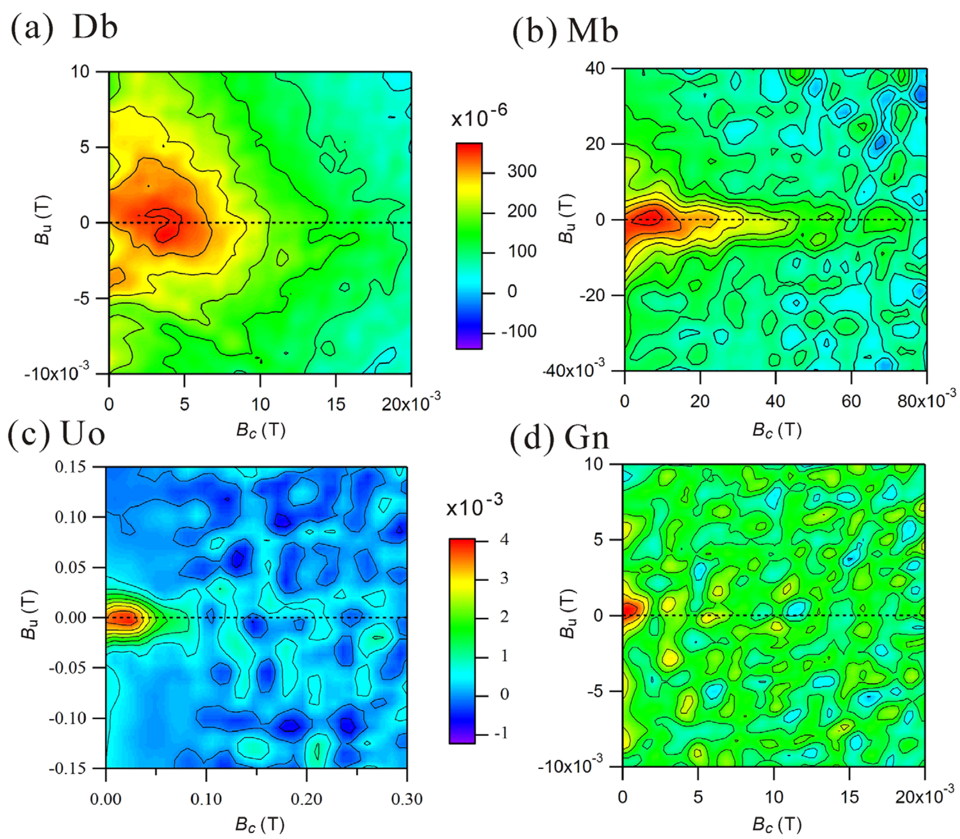

Figure 4. Typical FORC diagrams for selected samples from borehole ZK1, namely (a) Db, (b) Mb, (c) Uo, and (d) Gn. Data are analyzed with the software of FORCinel_1.18. All data are smoothed for identification, with SF (Smoothing factor) = 4 for Samples Db and Mb, SF = 5 for Uo, and SF = 6 for Gn, respectively.

Magnetic minerals with different coercivities and contents could be further distinguished by Lowrie's thermal demagnetization method in three-component IRM experiments [*Lowrie*, 1990] (Figure 6). For sample Db, all three components are fully demagnetized before 600°C (Figures 6a and 6e). The IRM demagnetization curves show a dominant soft (low-coercivity) component, with a moderate percentage of the medium and a few hard components. The medium and hard components increase as the alteration proceeds (i.e., samples Mb and Uo in Figures 6b and 6f, and Figures 6c and 6g, respectively), although the soft component still dominates the magnetization. Sample Gn consists of much more medium and hard magnetic components (Figures 6d and 6h), with fewer soft magnetic minerals.

The Verwey transition is an inherent property of magnetite and is also affected by the grain size [*Verwey*, 1939]. Low-temperature magnetic measurements (Figure 7) show distinct drops for all samples at ~120 K, except for sample Mb (Figure 7b). The first derivatives (d*M*/d*T*) of the thermal demagnetization curves of low-temperature remanence were calculated to better identify the changes during warming. The magnitude of the decline for sample Mb is principally apparent at ~30 K. For sample Uo (Figure 7c), the remanence displays a gradual decline throughout the variation of temperature, in addition to the distinct drops at ~30 and ~120 K. The low-temperature SIRM of sample Gn (Figure 7d) resembles that of sample Db (Figure 7a), but had much less magnetization.

4.2. Paleomagnetic Results

As the specimens were drilled from unoriented boreholes, the paleomagnetic results can only validate the stability of remanence. In Figure 8, most samples consist of more than one magnetic component. The NRM of sample Db (Figure 8a) is dominated by a low-coercivity component, which is demagnetized at a field of ~20 mT. The directions of the medium-coercivity (20–50 mT) and high-coercivity (>50 mT) components are scattered. The soft component remains the dominant remanence for sample Mb (Figure 8b), as nearly 90%

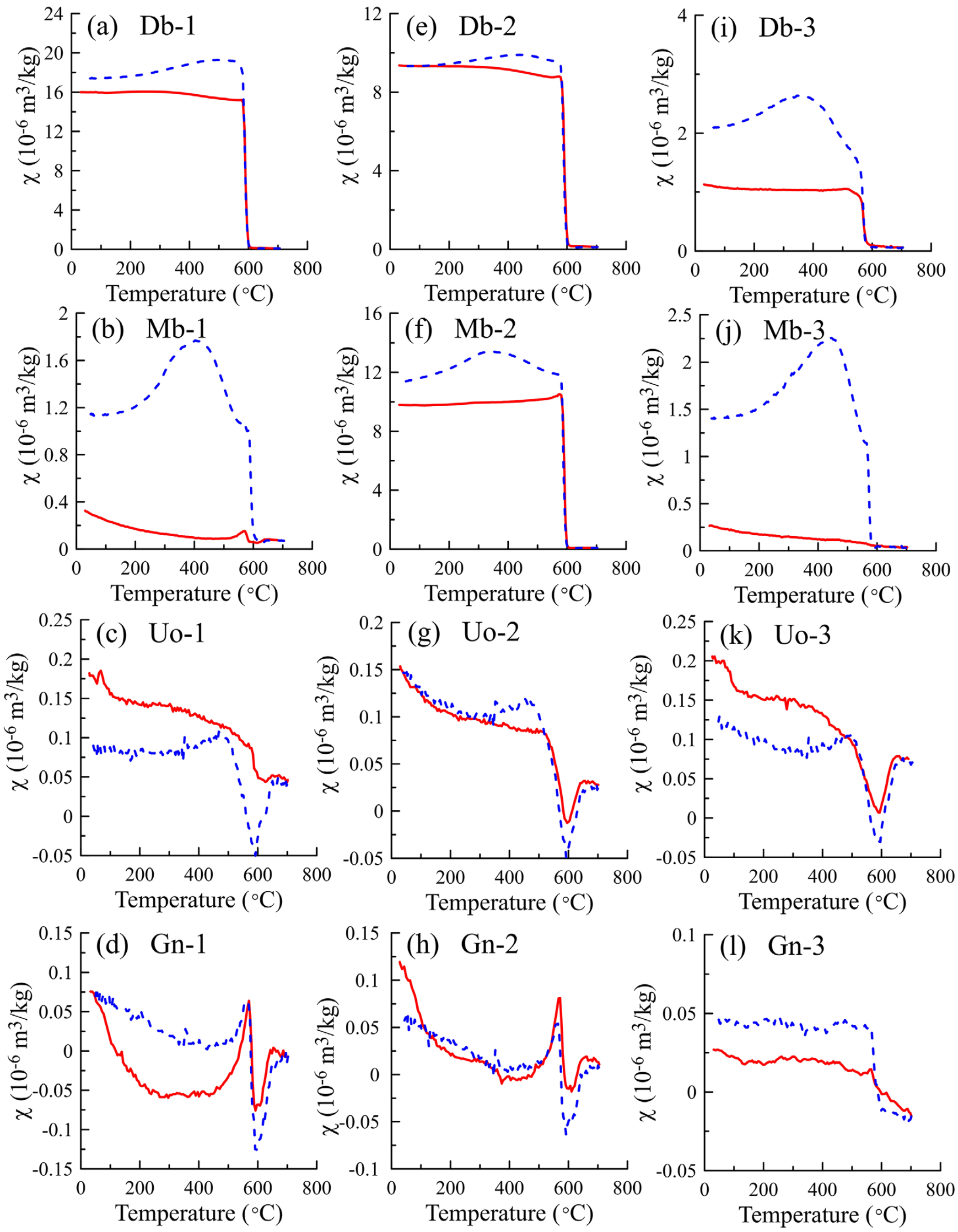

Figure 5. Temperature-dependence of magnetic susceptibility for selected samples from boreholes ZK1, ZK2, and ZK4, namely (a, e, and i) Db, (b, f, and j) Mb, (c, g, and k) Uo, and (d, h, and l) Gn. The heating curves and cooling curves are showed in solid and dashed lines, respectively.

of the NRM is demagnetized at a field of $\sim$15 mT. As with sample Db, sample Mb consists of very scattered remanence at a higher demagnetizing field.

The demagnetized behavior of sample Uo (Figure 8c) is much different. The directions of the low-coercivity and medium-coercivity components do not change much until the AF field is more than 50 mT. In contrast to the low-coercivity and medium-coercivity counterparts, the high-coercivity component occupies a large part of the NRM, and is not totally demagnetized at a field of 80 mT. Like samples Db and Mb, the NRM of sample Gn (Figure 8d) is dominated by the low-coercivity and medium-coercivity components.

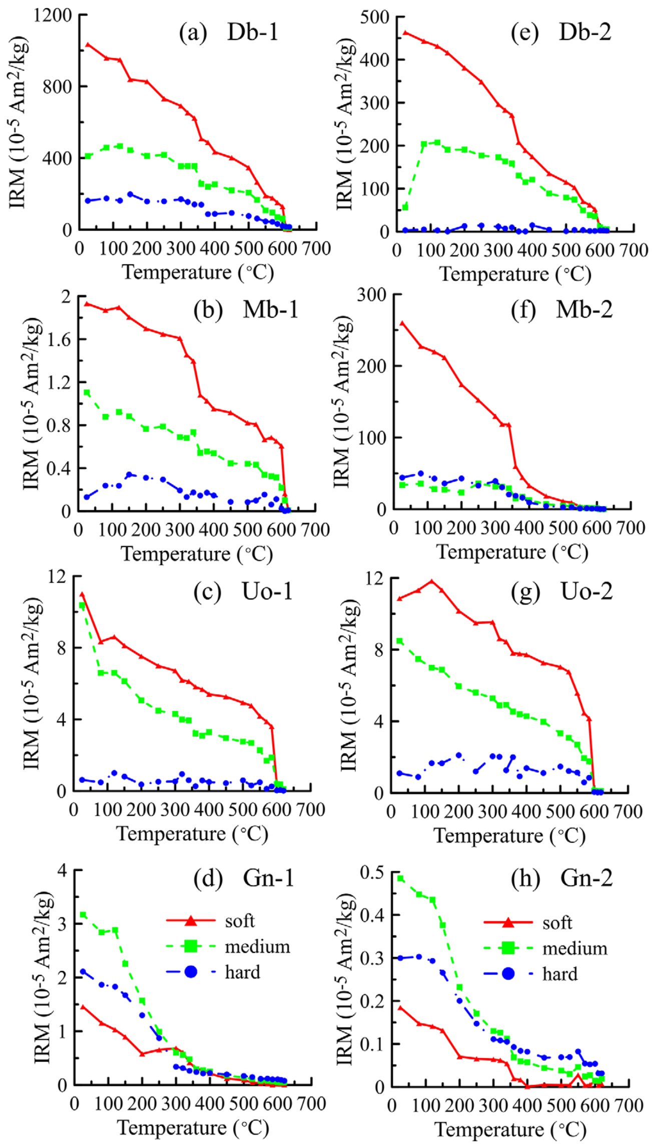

Figure 6. Thermal demagnetization of three-component IRM of typical samples from boreholes ZK1 and ZK2, namely (a and e) Db, (b and f) Mb, (c and g) Uo, and (d and h) Gn. The data were produced by magnetizing the samples in 2.5 T along their *z* axis, followed by 0.5 T along the *y* axis, and finally 0.15 T along the *x* axis.

4.3. Mineralogy Investigation

Microphotograph results of magnetic minerals display systematic changes in mineralogy for selected samples (Figure 9). The diabase sampled near the uranium belts (i.e., sample Db, Figure 9a) appears to have a certain degree of amphibolitization under regional metamorphism. Magnetite grains with a size of $\sim$100 μm (MD size) are precipitated from hornblendes (Figure 9a′). Compared with the magnetic minerals contained in sample Db, it is notable that the grain size of magnetite in sample Mb is remarkably smaller, with the occurrence of pyrites (Figure 9b′). In Figure 9c′, magnetite and pyrite grains in sample Uo are much finer and poorly crystallized. The microstructure of sample Gn (Figures 9d and 9d′) shows typical characteristics of monzonitic two-mica granite.

In summary, the vein-type uranium deposit displays four categories of behaviors for magnetic minerals during contact metamorphism:

Type 1: Sample Db displays a pseudo-single domain (PSD) or multidomain (MD) behavior of magnetite after a paramagnetic correction (Figures 3e and 4). It may also contain harder magnetic minerals, such as hematite (Figure 3i). The remanence was mostly recorded by soft magnetic minerals (probably MD magnetic particles as shown in Figure 5) with a demagnetizing field less than 20 mT. The remanence recorded by medium and hard minerals (probably hematite) is weak and scattered (Figures 6 and 8).

Type 2: Compared with the sample Db, sample Mb exhibits magnetic behaviors characteristic of finer magnetic and less concentrated particles (Figures 3 and 4). Hard magnetic minerals such as hematite can hardly be detected (Figure 3j). Differences of the χ-T curves for samples from different boreholes suggest variations and inhomogeneities due to alteration effects. The generation of new magnetic minerals deduced by the cooling curve of sample Mb indicates the instability of the altered diabase samples (Figures 5b, 5f, and 5j). Iron sulfide (e.g., pyrrhotite) is validated by the decrease of remanence at $\sim$350°C in Figure 6, and in the low-temperature SIRM curve of sample Mb (Figure 7), where a phase transition drop of remanence occurs at $\sim$30 K [*Dunlop and Özdemir*, 2001]. Meanwhile, the paramagnetic pyrites were directly observed by microscope observation (Figure 9). Magnetic recording behaviors of Mb is similar to that of sample Db, which is almost totally demagnetized at a low AF demagnetized field (Figure 8).

Type 3: Magnetic properties of sample Uo are complicated but of paramount importance to uncover the physicochemical alteration during the mineralization process. The wasp-waisted shapes of the hysteresis loops arise from the coexistence of two different magnetic components with contrasting coercivities

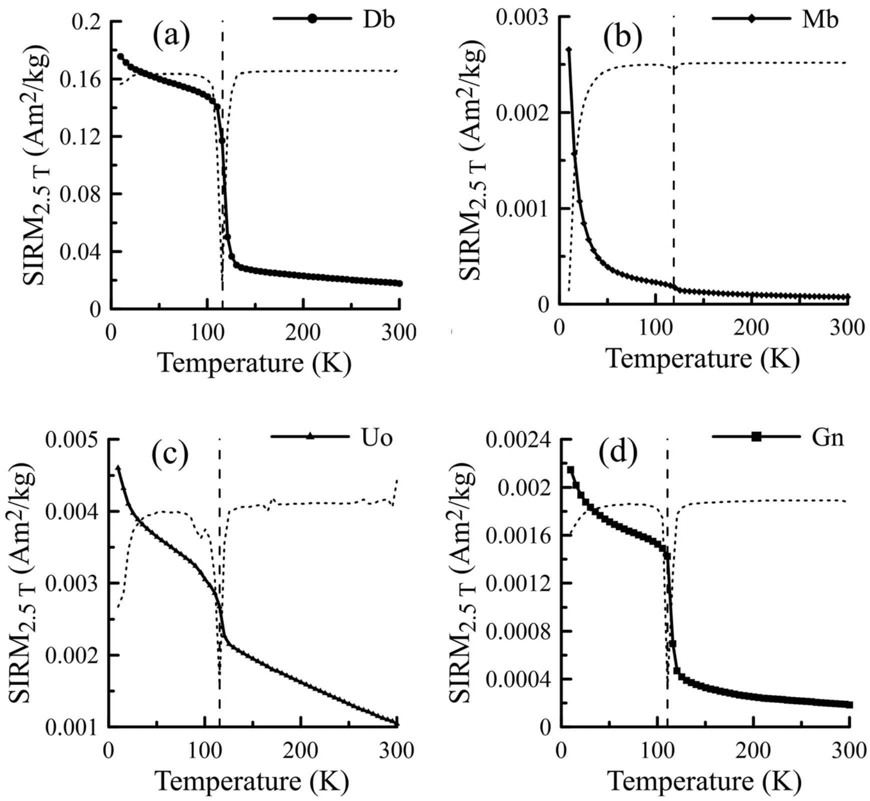

Figure 7. Low-temperature magnetic measurements for typical samples from borehole ZK1. Symbols indicate thermal warming from 10 to 300 K of the $SIRM_{2.5\ T}$, which is acquired with a field of 2.5 T at 10 K after cooling from 300 K (room temperature) in zero field. The dashed lines are the first derivatives of the thermal demagnetization curves, which indicate the Verway transition at ~120 K of magnetite.

(Figures 3g and 3k), probably the combination of low-coercivity magnetite and/or maghemite mixed with high-coercivity hematite [*Roberts*, 1995; *Tauxe et al*., 1996]. For the magnetite component, this type displays a SD behavior mixing with SP particles (Figures 3 and 4). In addition, the drop in remanence at ~30 K suggests the presence of pyrrhotite, but far less than that of sample Mb. Finer magnetite and paramagnetic pyrites are detected by microscope observation (Figure 9). Paleomagnetic results shows sample Uo consists of minerals with higher value of coercive field spectrum, indicating the existence and importance of NRM.

Type 4: As the sample from the wall rock in Xiazhuang area, sample Gn is magnetically weak (Figure 3). The FORC diagram (Figure 4d) and Hopkinson peak (Figures 5d, 5h, and 5l) demonstrate the existence of relatively few finer magnetite particles. The NRM of sample Gn is mostly demagnetized at a relatively low field, indicating magnetic minerals with lower values of coercive field spectrum (Figure 8).

4.4. Modeling Results

Magnetic properties linked with magnetic prospecting (Figure 2) have shown that susceptibility (χ) decreases by nearly a factor of 3 from sample Db to sample Mb. In contrast, the Koenigsberger ratio Q is significant higher for sample Uo, in comparison with sample Db and Mb. Sample Uo displays smaller χ and quantitatively fewer paramagnetic minerals (Figure 3c), suggesting a large decrease in the amount of magnetic recording minerals at the center of the intersection zone. The value of Q for sample Uo is relatively high, resulting in a comparable remanence relative to its induced magnetization. Compared with sample Uo, sample Gn shows decreased susceptibility (by ~50%) and lower Q value. Overall, the total magnetization decreased gradually from samples Db to Gn.

As is shown in Figure 10a, the first model describes a diabase dyke with a thickness of 10 m that is oriented in a NWW direction (Figure 1). In general, mafic dykes (e.g., sample Db in this study) display relatively large values of magnetization, resulting in high magnitude and gradient of magnetic anomalies (Figure 10a′), even in areas with igneous wall rocks (e.g., sample Gn in this study). The second model displays exactly the

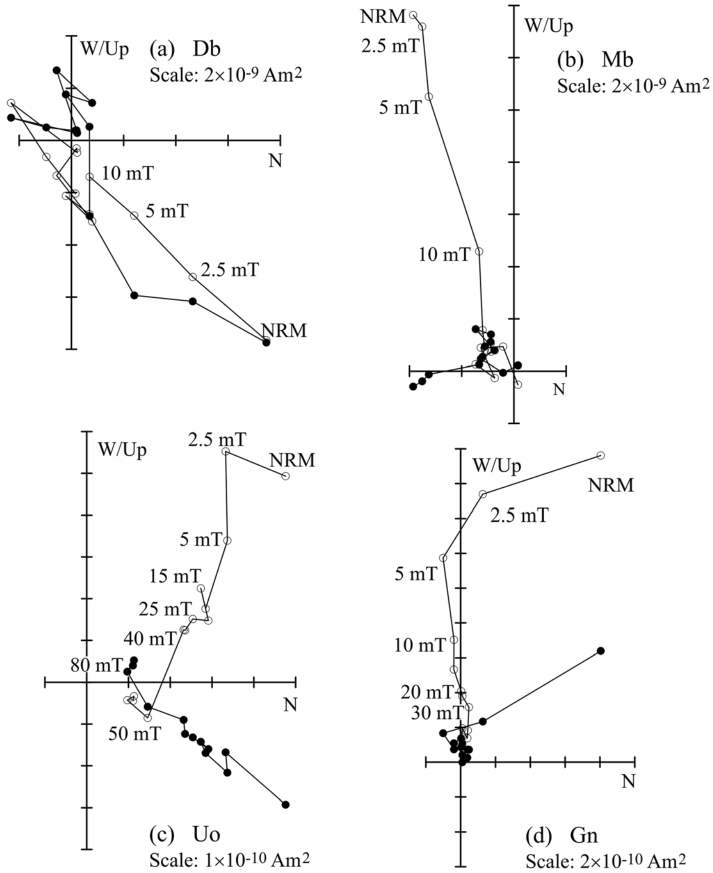

Figure 8. Representative orthogonal plots of remanence versus field of AF demagnetization of typical samples from borehole ZK1.

same diabase dyke intersected by a 10 m thick silicified fault (Figure 10b). In the model, the silicified fault has the characteristics of the meta-diabase (Mb), a decreased susceptibility and NRM (Figure 10b′). This will give rise to relatively negative and low-gradient magnetic anomalies, resulting in the "demagnetization effect" [*Min et al.*, 2005; *Li et al.*, 2012]. Combined with other efficient exploration methods, it is possible to estimate the vein-type uranium ore by figuring out the "demagnetized screening" part, using high resolution magnetic surveys.

Models in Figures 10c and 10d display intersections of the diabase dyke and silicified faults that host uranium deposits, both with thicknesses of 6 m and depths of 0 m and 100 m, respectively. Compared with Figure 10b′, the "demagnetized belt" in Figure 10c′ shows different magnetic characteristics, the magnetic anomalies of which quickly decreases to much lower values. However, for the uranium deposit that occurs deeper underground (Figure 10d), the gradient of the decrease for the magnetic anomalies vanishes, resembling the behaviors of the second model (Figure 10b).

5. Discussions

5.1. Implications for Metallogenic Environment

In nature, uranium usually migrates in the form of compounds or complexes that contain U^{6+}, and is reduced to a water-indissoluble form (U^{4+}) in an anoxic environment [*Wang et al.*, 2010]. Therefore, uranium deposits are produced in redox systems [*Castor and Henry*, 2000], which could be due to hydrocarbon leakage, rising of reducing gas, or reductive carbonized plants [*Pownceby and Johnson*, 2014].

The mineralogy of redox zones in areas of uranium deposits has been studied since the 1970s [*Shenoy et al.*, 1972; *Wachter and Cremers*, 1987; *Ge et al.*, 2014], using different physicochemical methods (e.g., Mössbauer spectroscopy, infrared spectrum analysis, electronic probe, X-ray diffraction). In particular, numerical studies have shown that mineral composition varies with the formation time and the distance from the center of the veins [*Min et al.*, 2005; *Wang et al.*, 2010; *Boyle*, 2013].

As the common metallic elements in the crust, compounds of iron like magnetite, pyrite, and hematite, often occurred with mineralization [*Dunlop and Özdemir*, 2001]. Environmental changes from strongly oxidizing to highly reducing are often accompanied by changes in the Fe-bearing minerals in a rock. Therefore, the redox environment of uranium can be characterized by the existing states of magnetic minerals.

In Xiazhuang area, as the concentration-related magnetic properties of rocks decrease from diabase to metamorphosed diabase and uranium ore, the total magnetization unambiguously decreases (Figure 2). This may arise from the metasomatism activities during the physicochemical alteration of hydrothermal fluid, such as chloritization and pyritization (Figures 6 and 9). Ferromagnetic minerals are altered to hematite,

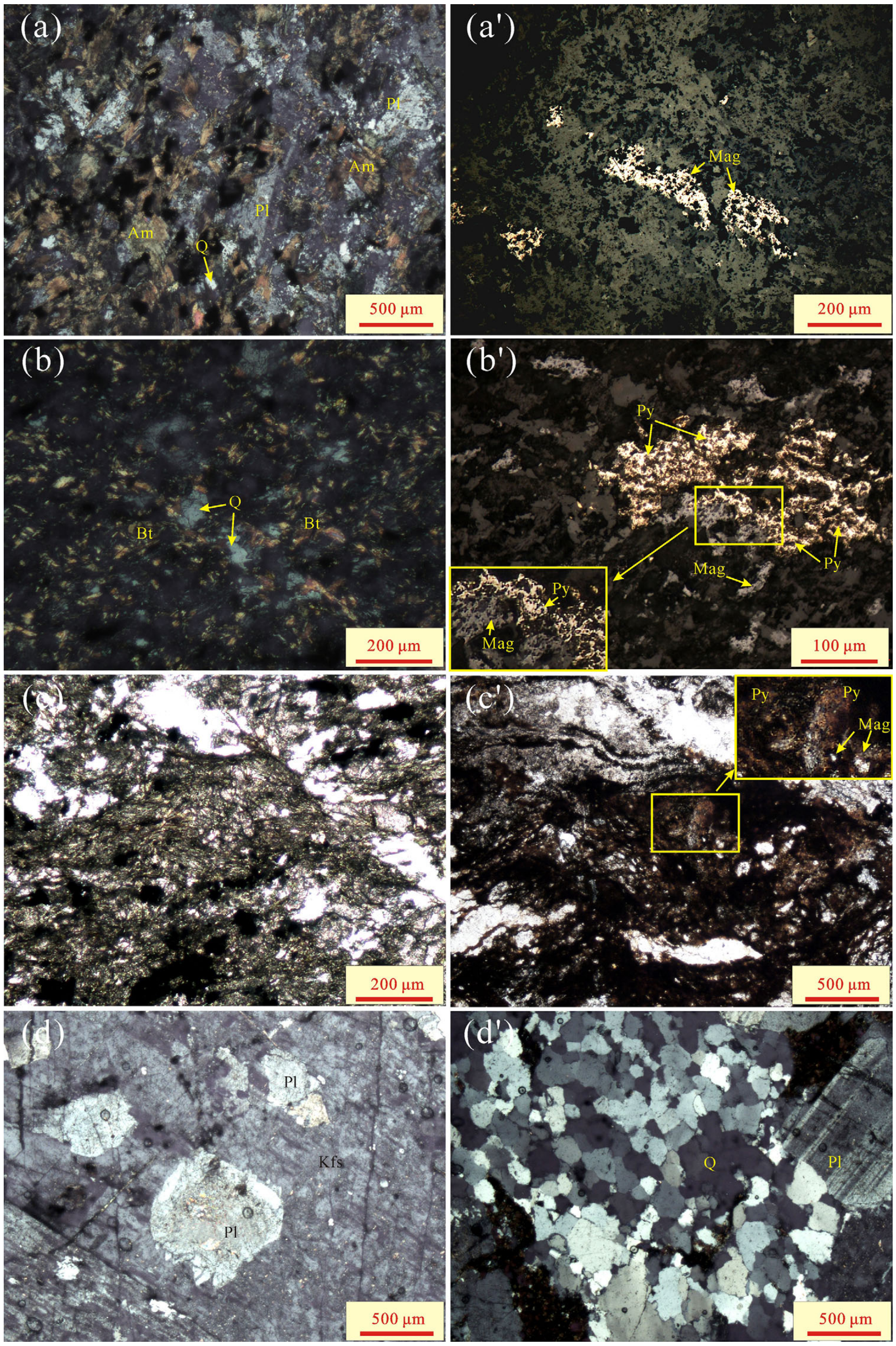

Figure 9. Representative microphotographs of typical samples from borehole ZK1, namely (a and a′) Db, (b and b′) Mb, (c and c′) Uo, and (d and d′) Gn. Figures (a and b′) for samples Db and Mb are viewed in reflected light, and Figures (c and d′) for samples Uo and Gn are in transmitted light. Selected areas in (b′ and c′) are amplified in the subfigures for illustrative purpose. Abbreviated symbols for rock-forming minerals are as follows, Am = Amphibole, Bt = Biotite, Kfs = K-feldspars, Mag = Magnetite, Pl = Plagioclase, Py = Pyrite, Q = Quatz.

pyrrhotite, pyrite, and other finer-grained magnetic particles, resulting in variations in the magnitude of magnetization. For instance, the specimen consisting of uranium ore (sample Uo) displays increased coercivity and higher destructive field, resulting from the finer-grained magnetic particles generated from metasomatism.

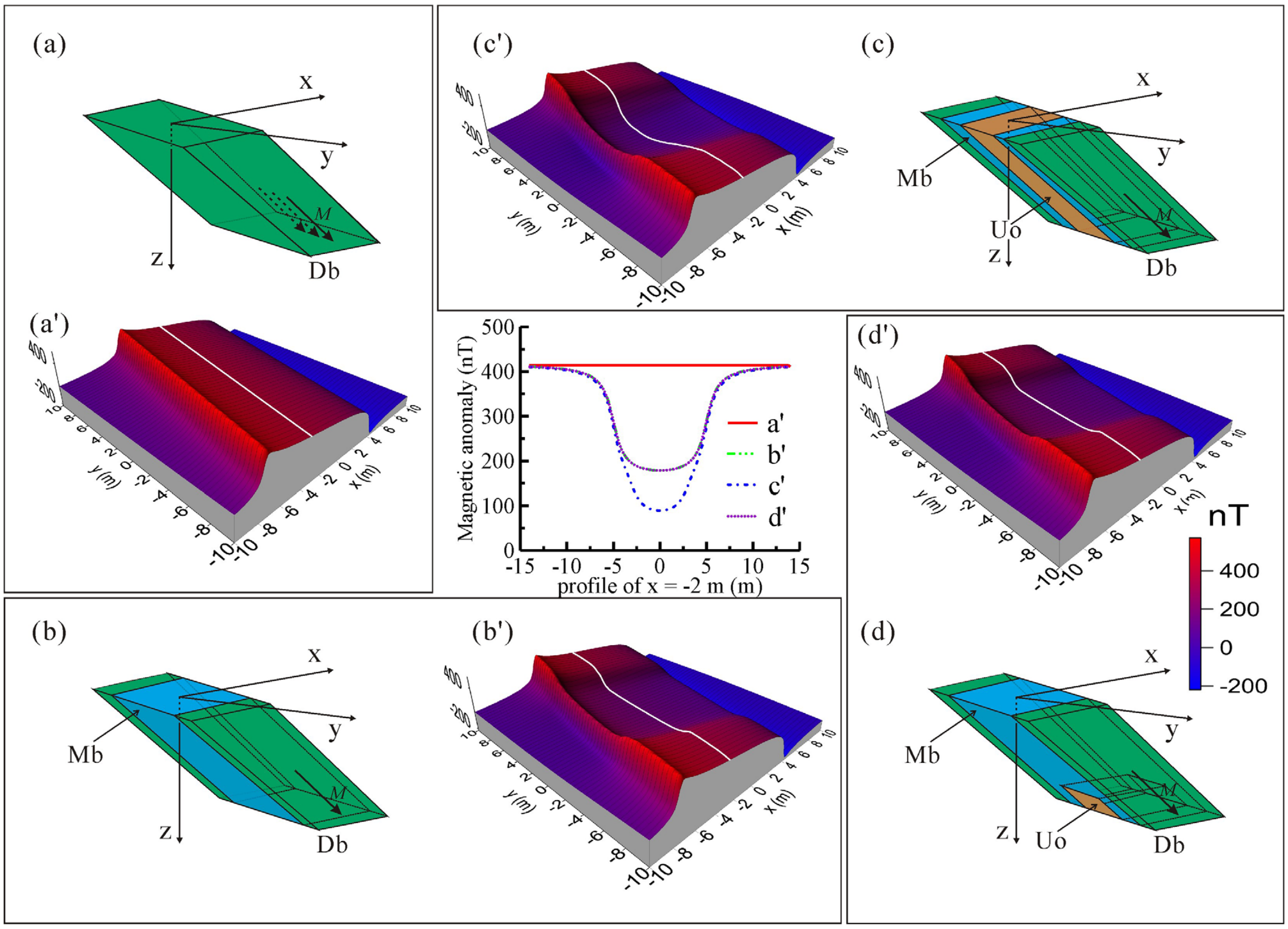

Figure 10. Magnetic models (a–d) and magnetic anomalies (a′–d′) of modeling (a) a bedding magnetized diabase dyke with infinite extension in both strike and depth, (b) a bedding magnetized diabase vertically intersected by a silicified zone, (c) an intersection of a diabase dyke and a silicified zone that contains a surfaced exposed uranium deposit, and (d) an intersection of a diabase dyke and a silicified zone that contained a uranium deposit 100 m underground, respectively. The outlines of magnetic anomalies (a′–d′) at $x = -2$ m are shown in white lines, and summarized in the central subfigure.

The diabase provides a redox transitional zone, which is characterized by iron oxides in this study. Ferrous compounds and hydrogen sulfide in mafic dykes form the redox environment, reducing and enriching the uranium from passing hydrothermal fluids. The uranium ore bodies finally fill the breccia voids of mafic dykes or intersections near fracture zones, in the form of veins and veinlets.

5.2. Implications for Magnetic Exploration

Traditional magnetic surveys attempt to find the "demagnetized belt" (Figure 10b′) during the investigations of vein-type uranium deposit [*Min et al.*, 2005]. However, as has been shown in our research, two important issues should be seriously considered. First, poor investigations of the properties of rocks could mislead the geophysical interpretation based only on anomalies at the surface. More systematic analyses of magnetic properties should be conducted to contribute to the magnetic survey of uranium deposits. Second, two morphologies of the "demagnetized belt" that host uranium deposits are found in this study. (i) The high-gradient decrease of magnetic anomalies in intersection zones indicates a strong metamorphism that hosts shallow uranium deposits. Combined with the radioactivity prospecting methods, the position of orebodies can be well located. (ii) The low-gradient decrease of magnetic anomalies suggesting the nonexistence of a uranium deposit (Figure 10b) or more deep hosted orebodies (Figure 10d). This would be an important characteristic for finding more vein-type uranium deposits, as not all intersection zones of dibase dykes with silicified faults in granite possess uranium ore [*Castor and Henry*, 2000]. Meanwhile, it is considered that integrated geophysical methods (e.g., combination of magnetic survey and magnetotellurics) should be conducted in hunting for deep vein-type uranium orebodies.

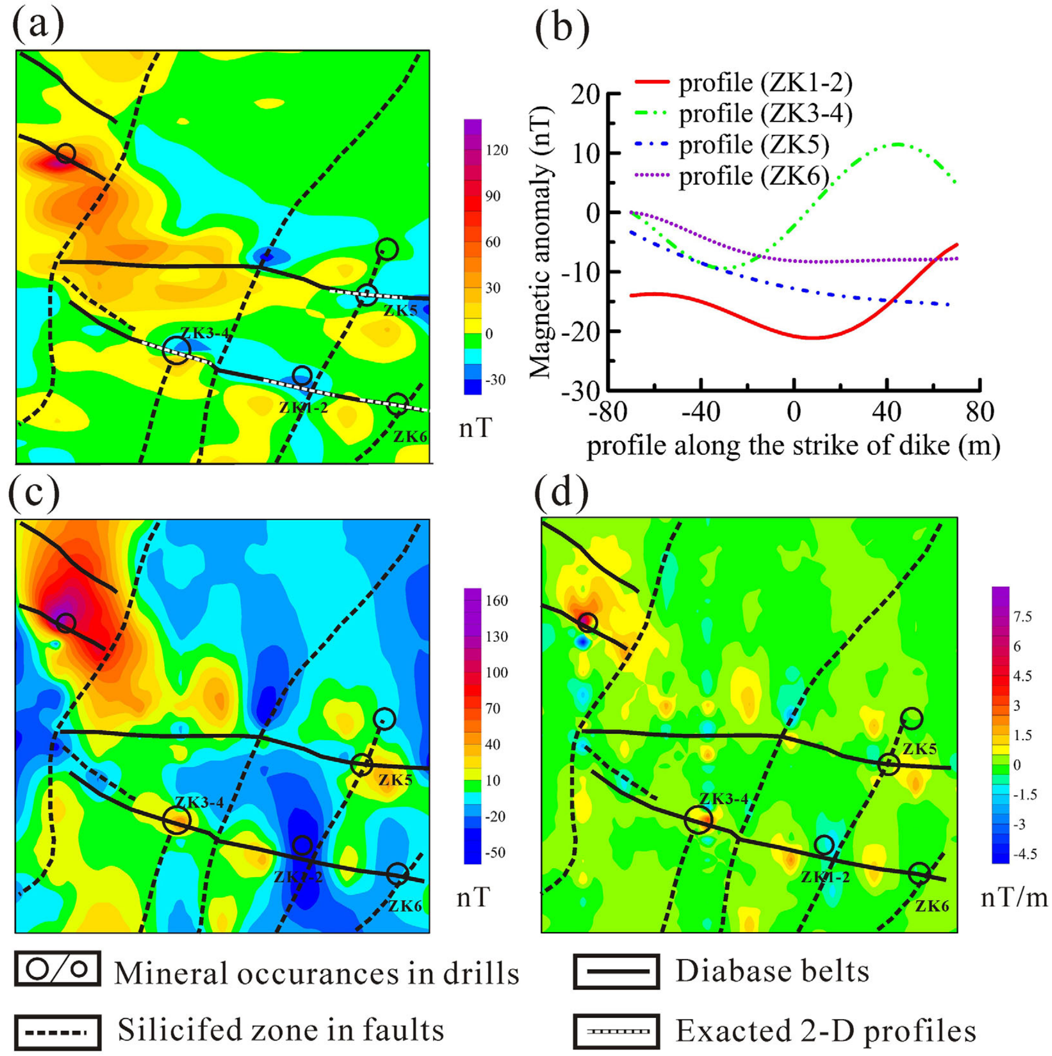

Figure 11. Contours of magnetic anomalies (a, c, and d) of the selected area (the dash square in Figure 1) and extracted 2-D profiles (b) of mapping diabase dyke around boreholes. (a) original magnetic anomaly (after correction of diurnal variation and extraction of IGRF 11); (b) anomalies of extracted 2-D profiles from Figure 11a; (c) anomaly (Figure 11a) after reduction to the pole; (d) map of the first-order derivative of reduced anomaly (Figure 11b) in *Z* direction.

Magnetic survey data over the sampling location were collected by surface magnetic survey in 2014, using ENVI PRO Proton Magnetic System (Scintrex Ltd., Concord, Canada) and Garmin GPS (Garmin E-Trex Legend, Garmin International, Inc., Olathe, USA). The grid spaces of magnetic survey are 100 m along the north direction and 20 m along the east direction, respectively. Original data were then smoothed and processed into a grid of 25 m $\times$ 25 m for further calculations [*Krige*, 1951]. As are shown in Figure 11a, the outlines of diabase dykes are basically determined by positive magnetic anomalies. The NNE aligned silicified faults mostly display relatively low magnetic anomalies when cross-cutting the diabase dyke, resembling the trend of modeling results in Figure 10. Magnetic anomalies of the extracted 2-D profiles decrease around boreholes (situated at 0 m in Figure 11b), with an exception of borehole ZK5. Moreover, it seems that borehole ZK5 is also situated between magnetic highs, although the direction of which is not along the strike of mapped diabase (Figure 11a).

The method of reduction to pole based on the local magnetic field highlights several anomalies of the diabase dyke, e.g., the positive anomaly extended parallel with the diabase belt at the bottom of Figure 11c. The magnetic anomalies around most boreholes display relatively high-gradient decreases after reduction to the pole. In contrast, boreholes ZK3-4 are situated close to a magnetic peak. It is probably because the silicified fault does not pass over the diabase dike, resulting in high magnetic anomalies by unaltered diabase in the intersection zone. The first-order derivative of the reduced magnetic anomaly in *Z* direction signified the high-gradient decrease around boreholes (Figure 11d), especially for boreholes ZK1-2.

However, inconsistencies between forward modeling and magnetic surveys still exist, e.g., the quantity of magnetic anomalies in Figures 10 and 11. The magnitude and locations of magnetic anomalies for some diabase dykes were not as well improved as that for the other dykes, e.g., the misalignment of magnetic highs and diabase dykes (Figure 11c). This is probably due to the superimposed effect of magnetic anomalies, and the significant contribution of magnetic remanence (Figure 2d).

In magnetic exploration, magnetic signals generated by magnetized geological bodies will overlap with each other and produce indistinguishable results. Reduction to the pole is one of the indispensable links that transform magnetic anomalies arising from oblique magnetization to vertical magnetization, and potentially produce independent signals [*Hinze et al*., 2013]. However, without the accurate results of remanent magnetization M_r, reduction to the pole based on the local inclination, will only reduce the component of magnetic induction (M_i) to the pole. M_r, which is probably not in the same direction with the induced magnetization, will be erroneously reduced and yield questionable results. *Shearer et al*. [2005] has proposed that erroneous results could be produced when the magnetization direction is incorrectly estimated by more than 15° [*Baranov*, 1957; *Li and Oldenburg*, 1996]. This effect will be amplified in areas of magmatic rocks.

It is hence necessary to consider the influence of magnetic remanence, and reduction to the pole and other magnetic processes must refer to the accurate direction of magnetization. In comparison with numerical methods [*Dannemiller and Li*, 2006; *Gerovska and Araúzo-Bravo*, 2009; *Li et al*., 2010], the effect of magnetic remanence will be interpreted more directly and accurately by rock magnetic methods. Overall, the comprehensive analysis of magnetic properties is of great significance in the current interpretation for the magnetic exploration of uranium deposits.

6. Conclusions

Rock magnetic experiments on typical vein-type uranium ore and its preserving redox environment were systematically investigated. These results showed gradual variations of magnetic properties from rim to center of the vein, i.e., the stage of metamorphism. As the alteration proceeded, the domain states of magnetite particles changed from large PSD and MD to SP and SD, and the quantity of iron sulfide increased. In particular, the magnetic parameters fluctuated greatly in metamorphic diabase samples. Moreover, compared with the surrounding weakly metamorphic rocks, the magnetic remanence of uranium ore displayed much higher stability and value of the Koenigsberger ratio Q. The contribution of the intersection zone to magnetic anomalies was modeled, and the analyses of the magnetic properties of vein-type uranium deposits are significant for further developing magnetic exploration for uranium ore. The results provide new methods to evaluate the mineralization and exploration of vein-type uranium deposits.

Acknowledgments
All the new data and interpretations in this study have been uploaded into the MagIC database as private (http://earthref.org/MagIC/11773/). We first appreciate Yongjae Yu and an anonymous reviewer for their carful work and thoughtful suggestions that have improved this paper substantially. Junjie Sun and Jianxing Liu helped prepare the samples. We thank Greig Paterson for his instructive comments on the low-temperature magnetic measurements, and Shuhui Cai for her help in uploading the paleomagnetic and rock magnetic data. This work was supported by the Nuclear Power Development Project (NPDP grant 2013-969) and National Nature Science Foundation of China (NSFC grants 41504054 and 41504098). Kunpeng Ge further thanks to the Doctoral Scientific Research Foundation of ECUT (1410000102).

References

Baranov, V. (1957), A new method for interpretation of aeromagnetic maps: Pseudo-gravimetric anomalies, *Geophysics*, *22*, 359–382, doi: 10.1016/J.Physb.2005.10.076.

Bonnetti, C., M. Cuney, R. Michels, L. Truche, F. Malartre, X. D. Liu, and J. X. Yang (2015), The multiple roles of sulfate-reducing bacteria and Fe-Ti oxides in the genesis of the Bayinwula roll front-type uranium deposit, Erlian basin, NE China, *Econ. Geol.*, *110*, 1059–1081, doi: 10.2113/econgeo.110.4.1059.

Boyle, R. W. (2013), *Geochemical Prospecting for Thorium and Uranium Deposits*, pp. 16–36, Elsevier, Amsterdam.

Castor, S. B., and C. D. Henry (2000), Geology, geochemistry, and origin of volcanic rock-hosted uranium deposits in northwestern Nevada and southeastern Oregon, USA, *Ore Geol. Rev.*, *16*, 1–40, doi:10.1016/S0169-1368(99)00021-9.

Chen, Y. W., X. W. Bi, R. Z. Hu, and S. H. Dong (2012), Element geochemistry, mineralogy, geochronology and zircon Hf isotope of the Luxi and Xiazhuang granites in Guangdong province, China: Implications for U mineralization, *Lithos*, *150*, 119–134, doi:10.1016/j.lithos.2012.06.025.

Cuney, M., and P. Barbey (2014), Uranium, rare metals, and granulite-facies metamorphism, *Earth Sci. Front.*, *5*, 729–745, doi:10.1016/j.gsf.2014.03.011.

Cunningham, C. G., J. D. Rasmussen, T. A. Steven, R. O. Rye, P. D. Rowley, S. B. Romberger, and J. Selverstone (1998), Hydrothermal uranium deposits containing molybdenum and fluorite in the Marysvale volcanic field, west-central Utah, *Miner. Depos.*, *33*, 477–494, doi: 10.1007/s001260050164.

Dannemiller, N., and Y. Li (2006), A new method for determination of magnetization direction, *Geophysics*, *71*(6), L69–L73, doi:10.1190/1.2356116.

Dunlop, D. J., and Ö. Özdemir (2001), *Rock Magnetism: Fundamentals and Frontiers*, pp. 170–190, Cambridge Univ. Press, New York.

Enkin, R. J., and D. J. Dunlop (1987), A micromagnetic study of pseudo single-domain remanence in magnetite, *J. Geophys. Res.*, *92*, 12,726–12,740, doi:10.1029/JB092iB12p12726.

Ge, K. P., W. Wyn, Q. S. Liu, and Y. Yu (2014), Effects of the core-shell structure on the magnetic properties of partially oxidized magnetite grains: Experimental and micromagnetic investigations, *Geochem. Geophys. Geosyst.*, *15*, 2021–2038, doi:10.1002/2014GC005265.

Gerovska, D., and M. J. Araúzo-Bravo (2006), Calculation of magnitude magnetic transforms with high centricity and low dependence on the magnetization vector direction, *Geophysics*, *71*, 121–130, doi:10.1190/1.2335516.

Hill, M. J., and J. Shaw (1999), Palaeointensity results for historic lavas from Mt Etna using microwave demagnetization/remagnetization in a modified Thellier-type experiment, *Geophys. J. Int.*, *139*, 583–590, doi:10.1046/j.1365-246x.1999.00980.x.

Hinze, W. J., R. V. Frese, and A. H. Saad (2013),*Gravity and Magnetic Exploration: Principles, Practices, and Applications*, 41 pp., Cambridge Univ. Press, New York.

Hopkinson, J. (1889), Magnetic and other physical properties of iron at a high temperature, *Philos. Trans. R. Soc.*, *180*, 443–465.

Hrouda, F. (2011), Models of frequency-dependent susceptibility of rocks and soils revisited and broadened, *Geophys. J. Int.*, *187*, 1259–1269, doi:10.1111/j.1365-246X.2011.05227.x.

Hu, R. Z., C. Y. Li, S. J. Ni, J. Liu, and J. S. Yu (1993), Research on ΣCO2 Source in Ore-forming Hydrothermal Solution of Granite-Type Uranium Deposit, South China, *Sci China Ser. B*, *36*, 1252–1262, doi:10.1360/yb1993-36-10-1252.

Hu, R. Z., X. W. Bi, M. F. Zhou, J. T. Peng, W. C. Su, S. Liu, and H. W. Qi (2008), Uranium metallogenesis in South China and its relationship to crustal extension during the Cretaceous to Tertiary, *Econ. Geol.*, *103*, 583–598, doi:10.2113/gsecongeo.103.3.583.

Kirschvink, J. L. (1980), The least-squares line and plane and the analysis of paleomagnetic data, *Geophys. J. R. Astron. Soc.*, *62*, 699–718, doi:10.1111/j.1365-246X.1980.tb02601.x.

Koenigsberger, J. G. (1938), Natural residual magnetism of eruptive rocks, *Terr. Magn. Atmos. Electr.*, *43*, 299–320, doi:10.1029/TE043i003p00299.

Krige, D. G. (1951), A statistical approach to some mine valuations and allied problems at the Witwatersrand, master thesis, Univ. of Witwatersrand, Witwatersrand, South Africa.

Kruiver, P. P., M. J. Dekkers, and D. Heslop (2001), Quantification of magnetic coercivity components by the analysis of acquisition curves of isothermal remanent magnetization, *Earth Planet. Sci. Lett.*, *189*, 269–276.

Li, M., G. X. Fang, Z. Y. Zhang, and J. C. Cao (2012), The application of ground high-precision magnetic survey to the exploration of intersection-type uranium deposits [in Chinese with English abstract], *Geophys. Geochem. Explor.*, *36*, 355–359.

Li, Y., and D. W. Oldenburg (1996), 3-D inversion of magnetic data, *Geophysics*, *61*, 394–408, doi:10.1190/1.1443968.

Li, Y., S. E. Shearer, M. M. Haney, and N. Dannemiller (2010), Comprehensive approaches to 3D inversion of magnetic data affected by remanent magnetization, *Geophysics*, *75*(1), L1–L11, doi:10.1190/1.3294766.

Liu, C. Y., K. P. Ge, C. X. Zhang, Q. S. Liu, C. L. Deng, and R. X. Zhu (2011), Nature of remagnetization of Lower Triassic red beds in southwestern China, *Geophys. J. Int.*, *187*, 1237–1249, doi:10.1111/j.1365-246X.2011.05196.x.

Liu, Q. S., S. Gao, and Y. S. Liu (2000), Magnetic structure of the continental crust as revealed by the Wutai-Jining crustal cross-section in the North China Craton, *J. Geodyn.*, *29*, 1–13, doi:10.1016/S0264-3707(99)00064-2.

Liu, Q. S., A. P. Roberts, J. C. Larrasoana, S. K. Banerjee, Y. Guyodo, L. Tauxe, and F. Oldfield (2012), Environmental magnetism: Principles and applications, *Rev. Geophys.*, *50*, RG4002, doi:4010.1029/2012RG000393.

Lowrie, W. (1990), Identification of ferromagnetic minerals in a rock by coercivity and unblocking temperature properties, *Geophys. Res. Lett.*, *17*, 159–162, doi:10.1029/GL017i002p00159.

Marignac, C., and M. Cuney (1999), Ore deposits of the French Massif Central: Insight into the metallogenesis of the Variscan belt, *Miner. Depos.*, *34*, 472–504, doi:10.1007/s001260050216.

Min, M., H. Xu, J. Chen, and K. Fayek (2005), Evidence of uranium biomineralization in sandstone-hosted roll-front uranium deposits, northwestern China, *Ore Geol. Rev.*, *26*, 198–206, doi:10.1016/j.oregeorev.2004.10.003.

Nettleton, L. L. (1976), *Gravity and Magnetics in Oil Prospecting*, pp. 81–102, McGraw-Hill, New York.

Orozco, A. F., K. H. Williams, and A. Kemna (2013), Time-lapse spectral induced polarization imaging of stimulated uranium bioremediation, *Near Surf. Geophys.*, *11*, 531–544, doi:10.3997/1873-0604.2013020.

Powncebý, M. I., and C. Johnson (2014), Geometallurgy of Australian uranium deposits, *Ore Geol. Rev.*, *56*, 25–44, doi:10.1016/j.oregeorev.2013.07.001.

Reynier, N., R. Lastra, C. Laviolette, J. F. Fiset, N. Bouzoubaâ, and M. Chapman (2015), Uranium, cesium, and mercury leaching and recovery from cemented radioactive wastes in sulfuric acid and iodide media, *Minerals*, *5*, 744–757, doi:10.3390/min5040522.

Roberts, A. P. (1995). Magnetic properties of sedimentary greigite (Fe_3S_4), *Earth Planet. Sci. Lett.*, *134*, 227–236, doi:10.1016/0012-821X(95)00131-U.

Roberts, A. P. (2006), Characterization of hematite (alpha-Fe_2O_3), goethite (alpha-FeOOH), greigite (Fe_3S_4), and pyrrhotite (Fe_7S_8) using first-order reversal curve diagrams, *J. Geophys. Res.*, *111*, B12S35, doi:10.1029/2006JB004715.

Ruzicka, V. (1993), Vein uranium deposits, *Ore Geol. Rev.*, *8*, 247–276, doi:10.1016/0169-1368(93)90019-U.

Saunders, D. F., S. A. Terry, and C. K. Thompson (1987), Test of national uranium resource evaluation gamma-ray spectral data in petroleum reconnaissance, *Geophysics*, *52*, 1547–1556, doi:10.1190/1.1442271.

Shearer, P., E. Hauksson, and G. Lin (2005), Southern California hypocenter relocation with waveform cross-correlation, Part 2: Results using source-specific station terms and cluster analysis, *Bull. Seismol. Soc. Am.*, *95*, 904–915, doi:10.1785/0120040168.

Shen, N. H., and Guan Z. N. (1985) *Magnetic Prospecting*, pp. 182–185, Geol. Publ. House, Beijing.

Shenoy, G., M. Kuznietz, B. Dunlap, and G. Kalvius (1972), Hyperfine magnetic fields in cubic uranium compounds from ^{238}U Mössbauer spectroscopy, *Phys. Lett. A*, *42*, 61–62.

Shu, X. J. (2004), Application of gravimetric and aeromagnetic data to the study of uranium ore-formation of granite-type uranium deposits [in Chinese with English abstract], *Uran. Geol.*, *20*, 99–119.

Tauxe L., T. Herbert, N. J. Shackleton, and Y. S. Kok (1996), Astronomical calibration of the Matuyama-Brunhes boundary: Consequences for magnetic remanence acquisition in marine carbonates and the Asian loess sequences, *Earth Planet. Sci. Lett.*, *140*, doi: 10.1016/0012-821X(96)00030-1.

Tauxe, L., H. N. Bertram, and C. Seberino (2002), Physical interpretation of hysteresis loops: Micromagnetic modeling of fine particle magnetite, *Geochem. Geophys. Geosyst.*, *3*(10), 1055, doi:10.1029/2001GC000241.

Thompson, R., and F. Oldfield (1986), *Environmental Magnetism*, Allen Unwin, London.

Tuncer, V., M. J. Unsworth, W. Siripunvaraporn, and J. A. Craven (2006), Exploration for unconformity-type uranium deposits with audio magnetotelluric data: A case study from the McArthur River mine, Saskatchewan, Canada, *Geophysics*, *71*(6), B201–B209, doi:10.1190/1.2348780.

US Atomic Energy Commission (1974), *Fuels, Environmental Survey of the Uranium Fuel Cycle*, WASH-1248, Fuels and Materials Directorate of Licensing, Washington, D.C., April.

Verwey, E. J. (1939), Electronic conduction of magnetite (Fe_3O_4) and its transition point at low temperature, *Nature*, *144*, 327–328, doi:10.1038/144327b0.

Wachter, J., and D. Cremers (1987), Determination of uranium in solution using laser-induced breakdown spectroscopy, *Appl. Spectrosc.*, *41*, 1042–1048.

Wang, Z., Z. Li, L. Wu, and G. Chen (2010), Geochemical evidences for mantle-derived uranium metallogenesis: A case study of Xiaoshui intersection-type uranium deposit in Xiazhuang area [in Chinese with English abstract], *Uran. Geol.*, *26*, 24–34.

WoldeGabriel, G., et al. (2014), Characterization of cores from an in-situ recovery mined uranium deposit in Wyoming: Implications for post-mining restoration, *Chem. Geol.*, *390*, 32–45, doi:10.1016/j.chemgeo.2014.10.009.

Wu, X. M., Q. C. Liu, Y. X. Yang, J. Z. Deng, and Y. Chen (2003), The application of the soil natural thermoluminescence method to the prospecting for deep concealed uranium deposits in the Xiazhuang uranium orefield [in Chinese with English abstract], *Geophys. Geochem. Explor.*, *27*, 338–344.

Yang, S. L. (2009), Application of comprehensive geophysical prospecting survey of alkali metasomatic rock uranium in Xiazhuang orefield [in Chinese with English abstract], *Chin. J. Eng. Geophys.*, *6*, 497–502.

Zhu, R. X., et al. (2004), New evidence on the earliest human presence at high northern latitudes in northeast Asia, *Nature*, *431*, 559–562, doi:10.1038/nature02829.

Zijderveld, D. A. (1967), AC demagnetization of rocks: Analysis of results, in *Methods in Paleomagnetism*, edited by D. W. Collinson, K. M. Creer, and S. K. Runcorn, pp. 254–286, Elsevier, Amsterdam.